Preparation and Magnetic Properties of Cu Ni Al Ferrite Nanoparticles and Polypyrrole/$Cu_{0.5}Ni_{0.5}Al_{0.3}Fe_{1.7}O_4$ Composite

W.A. Gabr[1,2,*], E.H. El-Ghazzawy[1], S.A. Saafan[1], A.M. Hussein[2]

[1] Physics Department, Faculty of Science, Tanta University, 31527, Tanta, Egypt

[2] Basic Science Department, Faculty of Engineering, Misr University for Science and Technology, Egypt

Abstract

Nanostructure copper nickel aluminum ferrite samples ($Cu_{0.5}Ni_{0.5}Al_xFe_{2-x}O_4$, x=0, 0.1, 0.2, 0.3 and 0.4) have been synthesized by using the citrate precursor technique. Then, a PPy/$Cu_{0.5}Ni_{0.5}Al_{0.3}Fe_{1.7}O_4$ composite sample has been prepared by polymerization of polypyrrole (PPy) monomer in the presence of $Cu_{0.5}Ni_{0.5}Al_{0.3}Fe_{1.7}O_4$ nanoparticles. The characterizing techniques used in the present investigation are X-ray diffraction analysis (XRD), scanning electron microscopy (SEM), Fourier transform infrared spectrometry (FTIR) and vibrating sample magnetometer (VSM) measurements. The results have revealed the pure formation of the desired ferrite nanoparticles. The formation of PPy has been evidenced by FTIR. The lattice constant and the theoretical density D_x have been found to decrease by increasing the aluminum content, whereas the Debye temperature and the elastic moduli have increased. The SEM image of the composite has obviously clarified that the ferrite particles are dispersed nearly homogeneously in the polymer matrix. The hysteresis loops of all samples have proved that they can be classified as soft magnetic materials. Moreover, the saturation magnetization M_s of the ferrite series has been found to decrease with the increase in Al content and also has further decreased in the composite as expected. The coercivity H_c has low values in general. Moreover, its value of the composite is higher compared to that of the pure Cu Ni ferrite because the PPy increases the surface anisotropy, whereas it is almost equal to the coercivity of the Al containing ferrites, indicating some similarity of introducing Al and PPy to the material from the perspective of interruption of the ferrimagnetic order. The low coercivity of the samples are required in important devices which depend on soft magnetic materials such as switching devices and high frequency transformers.

Keywords :nanoparticles, magnetic properties, composites

PACS: 75.50.Gg, 81.07.Wx

1. Introduction

The use of polymer nanocomposite materials has been increased in technological applications because of the possibility of forming new materials with a wide variety of characteristics [1, 2]. These nanocomposites are expected to have combined properties that the individual constituents may not provide each alone [3]. They may find important fields of use such as in electromagnetic interference shielding, and electronic devices. Particularly, nano-particle ferrite/polymer composites are promising materials too in those mentioned above applications and also in other significant applications such as chemical and electrical energy storage devices and different types of sensors [4]. However, spinel ferrites are a huge category of ferrimagnetic materials that possess high resistivity, low-level eddy current losses, good magnetization, and an excellent chemical stability [5-7]. Ferrites in both bulk and nano forms have been widely researched for their useful applications beginning from transformer cores to permanent magnets and magnetic recording [8-10]. The unit cell of spinel ferrite is formed of 32 oxygen anions in cubic arrangement with metallic cations distributed in interstitial tetrahedral A-sites and octahedral B-sites. Various properties of spinel ferrite nanocrystals are influenced by cation types and their distribution [11]. $NiFe_2O_4$ is known to be an inverse spinel ferrite where half of the ferric ions fill the tetrahedral (A-site) and the rest of them are introduced in the octahedral (B-site) under thermal equilibrium conditions [12-14]. $CuFe_2O_4$ also belongs to the inverse spinel category [15].

The mixed Ni-Cu ferrite possesses electrical and magnetic properties of the two amazing ferrites: Cu ferrite which is one of the most interesting ferrites, where it may undergo a structural phase transition accompanied by a reduction in the crystal symmetry to tetragonal [16], and Ni ferrite which has remarkable electrical and magnetic properties that leaded to many technological applications for decades.

Ferrite nanoparticles can be synthesized by different methods, with a range of crystallite sizes between 1 to 100nm. The most used methods are sol-gel, co-precipitation and citrate precursor.

On the other hand, polymers are very appealing materials, as they include a wide scope of capacities and applications from insulators to even metals [1]. The polypyrrole (PPy) has been known as an environmental friendly polymer with a relative stability and adjustable conductivity. The PPy based nano- ferrite composites may offer advantages of light weight and useful electromagnetic interference (EMI) suppression properties. Manipulating the dopant levels and nanoparticles content has given a wide range of research possibilities [17-20]. Moreover, introducing Al ions in the ferrite nano-particles instead of iron ions may participate in the formation of lighter products and may enhance low loss applications.

Therefore, the aim of the present work is to use the citrate precursor technique to prepare Cu Ni $Al_xFe_{2-x}O_4$ nanoparticles as new compositions – as far as the authors know - to be studied and to choose one of the prepared compositions to be incorporated with PPy to prepare a composite having combined characteristics promising in electronics and EMI applications.

2. Experimental

2.1 Preparation of $Cu_{0.5}Ni_{0.5}Al_xFe_{2-x}O_4$ nanoparticles:

$Cu_{0.5}Ni_{0.5}Al_xFe_{2-x}O_4$ nano-particles, (x=0, 0.1, 0.2, 0.3, and 0.4) have been synthesized by using the citrate precursor auto combustion method [21, 22]. According to this method; the proper amounts of metal nitrates were dissolved in distilled water obtaining clear solutions. Then, they were mixed and stirred for 1 hr. The citric acid was added drop-wise to the mixture solution, with the molar ratio of metal nitrates: citric acid adjusted at 1:1. Ammonia was added until the PH has reached to about 12. The solution was heated under stirring up to 90°C to form a highly viscous gel, then evolved reddish brown color gases were observed and a tree-shaped structure was formed. The tree-shaped product collapsed to form ash powder of the desired nanoparticle ferrites.

2.2 Preparation of Polypyrrole:

A pure PPy sample has been synthesized by in-situ polymerization of pyrrole monomers (using $FeCl_3.6H_2O$ as an oxidizing agent) [18, 23]. 0.08M pyrrole has been dissolved in 25mm^3 of acetone and stirred for 30 minutes. Then 0.2M ferric chloride was added drop-wise to the pyrrole. The reaction was carried out for 3 hours under continuous stirring at room temperature. The resulting precipitate has been obtained by filtering and washing the suspension with distilled water and finally dried at 80°C for 3 h.

2.3 Preparation of PPy/$Cu_{0.5}Ni_{0.5}Al_{0.3}Fe_{1.7}O_4$ composite:

One composite sample PPy/$Cu_{0.5}Ni_{0.5}Al_{0.3}Fe_{1.7}O_4$ has been prepared by in-situ polymerization of pyrrole monomers in the presence of $Cu_{0.5}Ni_{0.5}Al_{0.3}Fe_{1.7}O_4$ nanoparticles; where 3 g of the ferrite nanoparticles and 0.9M of pyrrole monomers were suspended in 25 mm^3 of acetone solution and stirred for 1 hr to get well dispersed suspension. Then $FeCl_3 \cdot 6H_2O$ was dissolved in 25mm^3 of acetone and this solution was added drop wise to the suspension mixture under a constant stirring. The polymerization was allowed to proceed for 2 h at room temperature. The composite has been obtained by filtering and washing the suspension with distilled water, then dried at 80°C for 3 h.

3. Characterization

The structure and crystallite size of the pure ferrite samples and the composite sample have been investigated by X-ray diffraction (XRD) analysis. The average crystallite size (R) have been calculated using Scherrer's formula: [2]

$$R = \frac{0.9\lambda}{\cos\theta\beta_{1/2}} \qquad (1)$$

Where $\beta_{1/2}$ is the full width at half maximum of the peak presenting the principle plane (311). By using the interplanar distances (d) obtained from Bragg's law; $2d\sin\theta = n\lambda$; the lattice constant (a) of all the ferrite samples have been calculated.

Also, the porosity (P) of those samples has been calculated by using the equation:

$$P = 1 - \frac{D}{D_x} \qquad (2)$$

; where (D_X) is the X-ray density (theoretical density) of the sample given by the well-known relation: [7, 22]

$$D_x = \frac{8M}{Na^3} \quad (g/cm^3) \qquad (3)$$

; where (D) is the experimental density of the sample.

The IR spectra for all samples have been recorded in the range of 200-2000 cm^{-1} by the Fourier-transform infrared spectrometer.

Magnetic characterization of the investigated nanoparticles has been performed at room temperature by a lab-built vibrating sample magnetometer (VSM) [24] with a maximum magnetic field up to 8 kOe.

The average particle sizes of the samples have been measured using the images of a scanning electron microscope (SEM).

4. Results and discussion

4.1 XRD analysis

Fig.1 shows the XRD patterns of the $Cu_{0.5}Ni_{0.5}Al_xFe_{2-x}O_4$ ($0 \leq x \leq 0.4$) samples. The XRD patterns reveal the characteristic peaks of single-phase cubic spinel with no undesired lines corresponding to any other phase. The intensity peaks represent (220), (311), (400), (422), (511), (440) and (533) planes respectively.

The variation of the average crystallite size R (nm) of all samples and the lattice constant a (Å) with Al concentration is shown in Fig. 2. It is clear that the lattice constant decreases by increasing aluminum concentration as expected because of the difference in the ionic radii of aluminum and iron ions; where larger Fe^{3+} (0.645Å) ions have been replaced by smaller Al^{3+}(0.55Å) ions; therefore this observed decrease in lattice constant is expected. Similar trend had been observed and reported in other aluminum substituted ferrite systems [25, 26].

The hopping length is the central separation between neighboring cations. Therefore, the substitution of larger cations by smaller ones results in a decrease of the distance between the magnetic ions and consequently the hopping lengths decrease. This is what has been observed in the investigated samples. The hopping length, L, in the A-sites are labeled (L_{A-A}), and those in the B-sites (L_{B-B}) whereas for shared sites, (L_{A-B}). They can be calculated using the following relations [27, 28].

$$L_{A-A} = a\frac{\sqrt{3}}{4},\ L_{B-B} = a\frac{\sqrt{2}}{4} \text{ and } L_{A-B} = a\frac{\sqrt{11}}{8}$$

The obtained data are listed in Table1. These results although they are all having the same trend of the lattice constant (a), they will be very useful in interpreting the conductivity of the investigated materials in a soon future work.

Table1 The obtained distance between magnetic ions (hopping length) in the A-sites (L_{A-A}), B-sites (L_{B-B}), and shared sites (L_{A-B}).

X	L_{A-A} (Å)	L_{B-B} (Å)	L_{A-B} (Å)
0	3.624	2.959	3.469
0.1	3.612	2.949	3.459
0.2	3.606	2.944	3.453
0.3	3.601	2.941	3.448
0.4	3.586	2.926	3.434

The X-ray density D_x of all samples has been determined from the molecular weight and the volume of the unit cell by using relation (3).

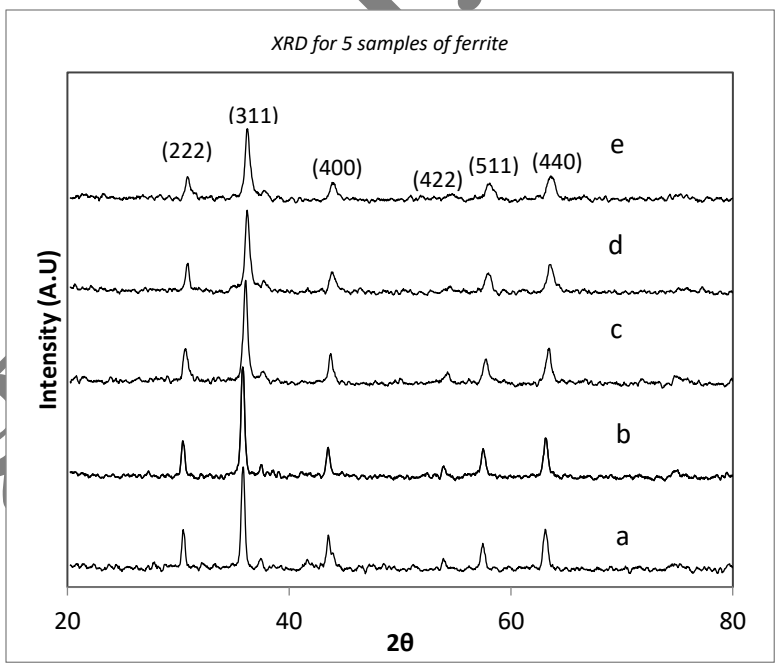

Fig. 1. XRD patterns of : (a) $Cu_{0.5}Ni_{0.5}Fe_2O_4$, (b) $Cu_{0.5}Ni_{0.5}Al_{0.1}Fe_{1.9}O_4$, (c) $Cu_{0.5}Ni_{0.5}Al_{0.2}Fe_{1.8}O_4$, (d) $Cu_{0.5}Ni_{0.5}Al_{0.3}Fe_{1.7}O_4$, (e) $Cu_{0.5}Ni_{0.5}Al_{0.4}Fe_{1.6}O_4$.

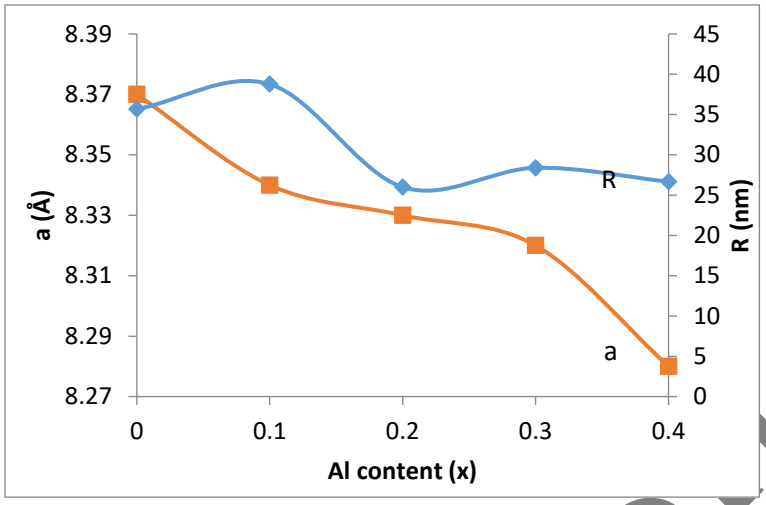

Fig.2. Variation of the lattice constant (a) and average crystallite size (R) against Al content (x) in the ferrite samples

Fig. 3. Shows the variation of the density D, X-ray density D_x and porosity P with aluminum concentration. D_x is found to decrease with increasing aluminum concentration. This can be attributed to the reduced molar mass of Al (26.98 gm mol^{-1}) compared with that of Fe (55.85 g mol^{-1}) [25]. Also from equation (3), the X-ray density is obviously dependent on the lattice parameter and the molecular weight of the samples [12].

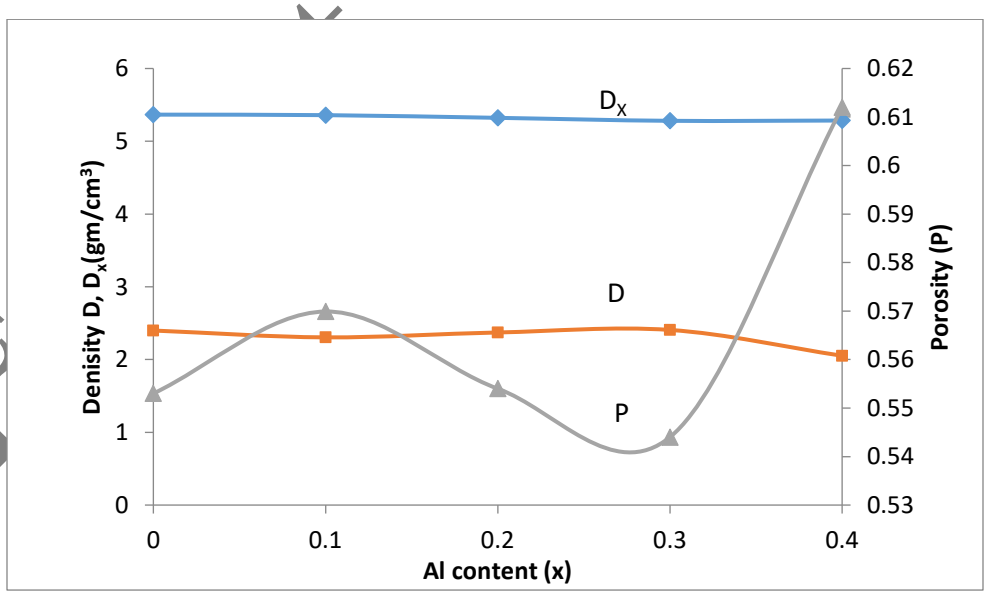

Fig.3. Dependence of density D, theoretical density Dx and porosity P on Al content (x) in the ferrite samples.

4.2 Morphology Investigation:

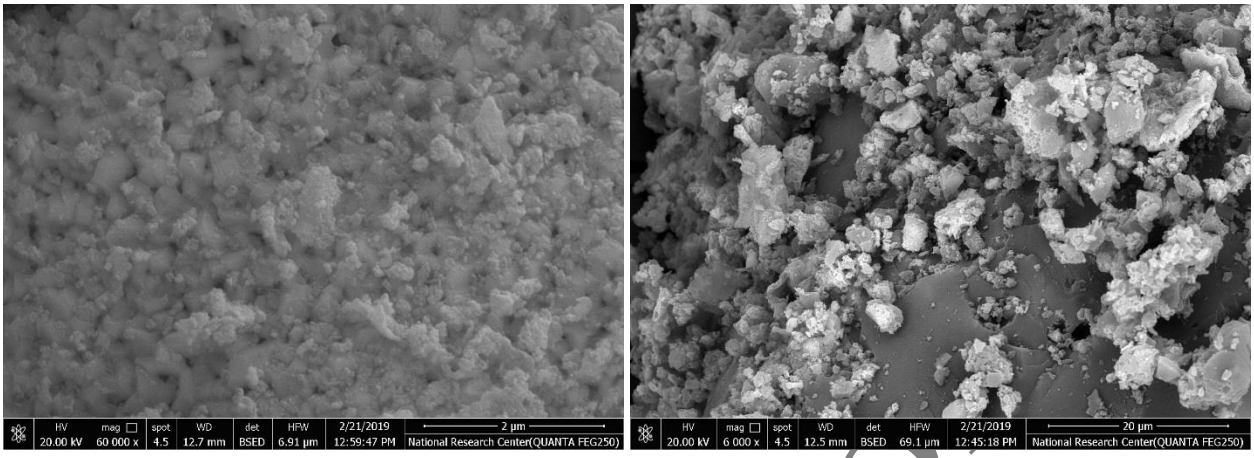

(a) (b)

Fig.4. SEM Images of (a) $Cu_{0.5}Ni_{0.5}Al_{0.3}Fe_{1.7}O_4$ nano-particles and (b) PPy/$Cu_{0.5}Ni_{0.5}Al_{0.3}Fe_{1.7}O_4$ composite.

Figures (4-6: a, b) show the SEM images of the as-prepared $Cu_{0.5}Ni_{0.5}Al_{0.3}Fe_{1.7}O_4$ nanoparticles and PPy/$Cu_{0.5}Ni_{0.5}Al_{0.3}Fe_{1.7}O_4$ composite A, respectively. The image (4-6a) shows that the ferrite nano-particles have a narrow particle size distribution. In image (4-6b), it is also seen that the $Cu_{0.5}Ni_{0.5}Al_{0.3}Fe_{1.7}O_4$ particles are dispersed nearly homogeneously in the polymer matrix. The average particle diameter has been estimated by using I image J software and has been found in the order of 26 nm which is in fair agreement with the value estimated from the XRD data.

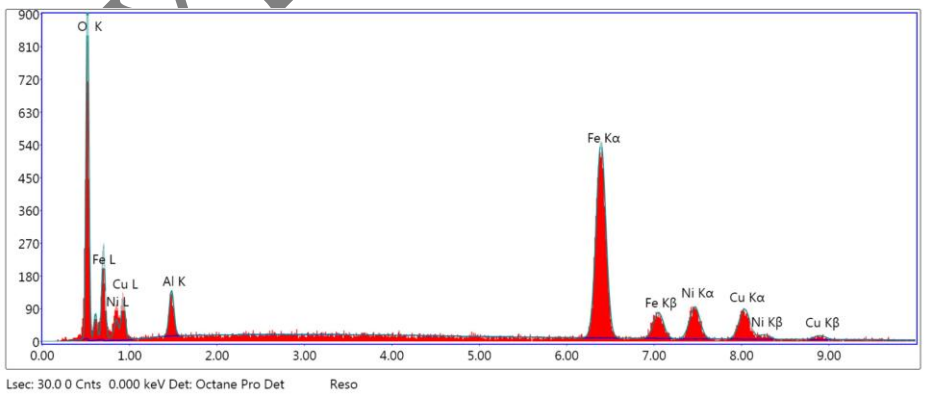

(a)

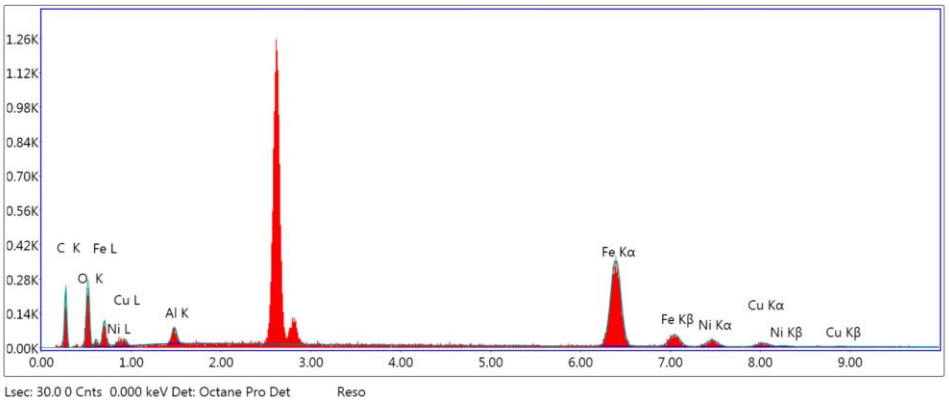

(b)

Fig.5. EDX for (a): $Cu_{0.5}Ni_{0.5}Al_{0.3}Fe_{1.7}O_4$ nanoparticles and (b): PPy/$Cu_{0.5}Ni_{0.5}Al_{0.3}Fe_{1.7}O_4$ composite.

Figures (5-7: a, b) display the EDX analysis of $Cu_{0.5}Ni_{0.5}Al_{0.3}Fe_{1.7}O_4$ and its composite (A) with PPy. The concentrations of different elements (Cu, Ni, Al, Fe, O and C) are listed in Tables (2: a, b). These concentrations are close to the desired ratio of the constituents of the prepared samples confirming the formation of the desired chemical composition.

Table (2a) EDX ratio of the components of $Cu_{0.5}Ni_{0.5}Al_{0.3}Fe_{1.7}O_4$ nanoparticles.

Element	Weight %	Atomic %	Net Int.	Error %
O K	21.13	47.83	129.45	7.91
Al K	3.74	5.03	27.7	12.62
Fe K	47.35	30.71	243.75	2.89
Ni K	12.57	7.75	43.38	8.5
Cu K	15.22	8.68	42.17	8.53

Table (2b) EDX ratio of the components of PPy/$Cu_{0.5}Ni_{0.5}Al_{0.3}Fe_{1.7}O_4$ composite.

Element	Weight %	Atomic %	Net Int.	Error %
C K	23.79	48.96	23.84	12.25
O K	14.83	22.91	37.4	11.6
Al K	2.73	2.5	16.4	14.68
Fe K	48.98	21.68	161.7	3.35
Ni K	5.62	2.37	12.9	17.91
Cu K	4.05	1.58	7.49	24.33

4.3 FTIR analysis

FTIR spectroscopy can detect the phases existing in a material as well as both chemical and structural changes. The room temperature FTIR spectra of the as-prepared $Cu_{0.5}Ni_{0.5}Al_xFe_{2-x}O_4$ nano- ferrites, PPy and PPy /$Cu_{0.5}Ni_{0.5}Al_{0.3}Fe_{1.7}O_4$ composite in the range 200-2000 cm^{-1} are depicted in Fig.6 (a, b) respectively.

All FTIR spectra reveal the presence of two major absorption bands, usually characterizing ferrites, at particular frequencies denoted by υ_1 and υ_2 [29]. The band at υ_1 in the range of 568-590 cm^{-1} is due to stretching vibrations of the tetrahedral A-site metal ion-oxygen bonds, and the band at υ_2 in the range of 384-397 cm^{-1} is attributed to vibrations of the octahedral B-site metal ion-oxygen bonds, these vibrations are known to be bond-bending vibrations [30]. The values of υ_1 are higher than those of υ_2, which show that the ordinary mode of vibration of the tetrahedral bonding is higher than that of the octahedral one indicating shorter bond lengths at the A-sites.

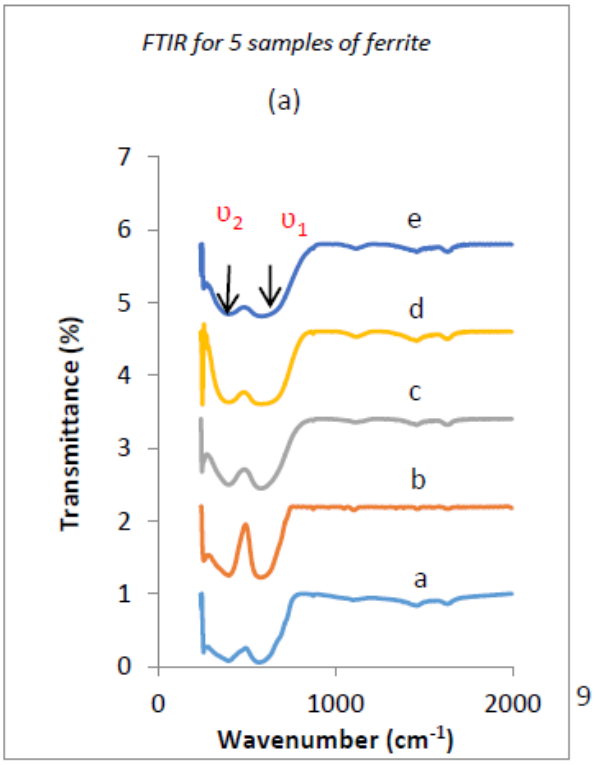

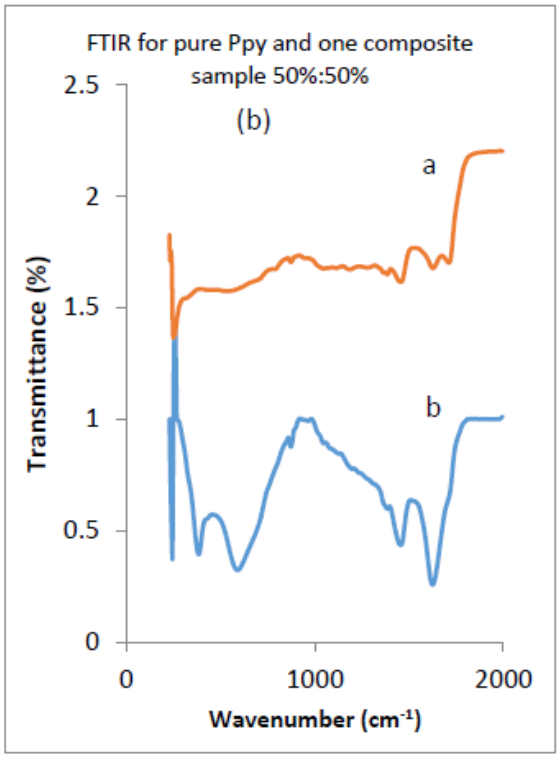

Fig.6. (a) FTIR of (a) $Cu_{0.5}Ni_{0.5}Fe_2O_4$, (b) $Cu_{0.5}Ni_{0.5}Al_{0.1}Fe_{1.9}O_4$, (c) $Cu_{0.5}Ni_{0.5}Al_{0.2}Fe_{1.8}O_4$, (d) $Cu_{0.5}Ni_{0.5}Al_{0.3}Fe_{1.7}O_4$, (e) $Cu_{0.5}Ni_{0.5}Al_{0.4}Fe_{1.6}O_4$.

(b) FTIR of (a) pure PPy and (b) PPy/$Cu_{0.5}Ni_{0.5}Al_{0.3}Fe_{1.7}O_4$.

From Table 3, it is observed that there is a slight movement in υ_1 absorption frequency towards a higher frequency accompanying the increase in the Al^{3+} ion concentration, whereas, such an increase is not observed in υ_2. This may be attributed to the shorter length of bonds at the tetrahedral sites is manifesting any change in the length of the bond -and consequently the vibration frequency -more than the longer bonds at the octahedral sites. This also refers to the difference in ionic radii of Fe^{3+} (0.645 Å) and Al^{3+} (0.55 Å) [29].

As a general definition of the force constant, it is the ratio between the force and the resulting deformation but only within elastic limits. The force constant here indicates somehow the origin of restricting the distances between nuclei at equilibrium during the vibrations of bonds at specific frequencies. F_A and F_B denote the force constants of the tetrahedral and octahedral sites, respectively. The force constants F_A and F_B vary with the corresponding bond length and the vibrational frequency (υ_1 and υ_2) according to:

$$F_A=4\pi^2c^2\,\upsilon_1^2\mu, \quad F_B=4\pi^2c^2\,\upsilon_2^2\mu,$$

; where μ is the reduced mass of $Fe^{3+}$and O^{2-}ions together ($\mu= 2.061\times10^{-23}$g) and c is the velocity of the electromagnetic wave [30]. Fig. 7 shows the variation of F_A and F_B with Al concentration.

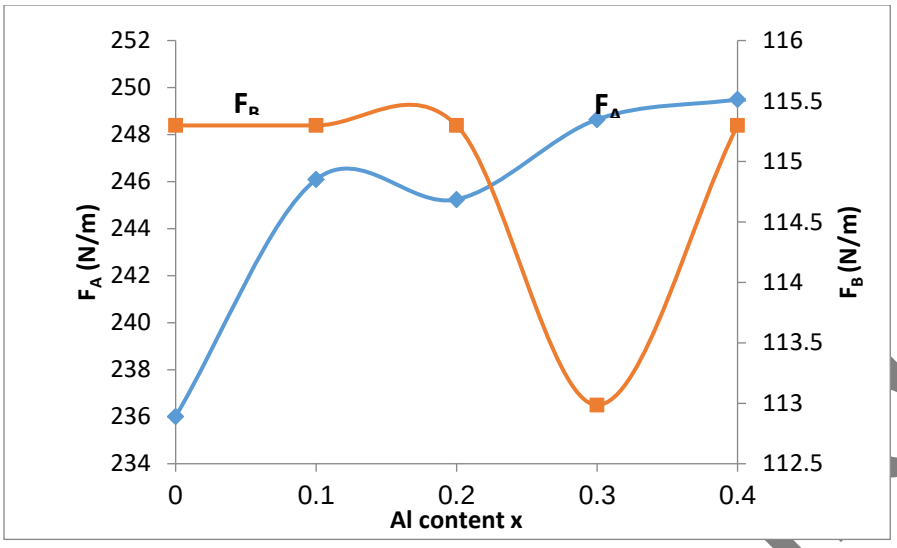

Fig.7. Force constants, F_A and F_B, at the A- and B-sites, as functions of Al content (x).

Table3. FTIR absorption band values and Force constants, F_A and F_B, at the A- and B-sites:

Sample	υ_1 cm^{-1}	υ_2 cm^{-1}	F_A(N/m)	F_B(N/m)	$F=(F_A+F_B)/2$
0	568	397	236.013	115.298	293.662
0.1	580	397	246.091	115.298	303.739
0.2	579	397	245.243	115.298	302.892
0.3	583	393	248.643	112.986	305.136
0.4	584	397	249.497	115.298	307.145
Composite A	590	384	254.650	113.562	311.430
Composite B	573	393	240.188	112.986	296.679

Fig.6 (b) represents the FTIR spectra of PPy and PPy /$Cu_{0.5}Ni_{0.5}Al_{0.3}Fe_{1.7}O_4$ composite, respectively. The characteristic absorption bands of polypyrrole [31] are observed at 896, 1400, 1471, 1639 and 1724 cm^{-1} in the figure. These absorption bands and their assignment are listed in Table. 3. The IR spectrum absorption peaks of PPy/ferrite composite are almost identical to those of PPy. However, υ_2 in the spectrum of the composite was slightly red shifted. It indicates that the bonds between the octahedral site ions and the oxygen ions have been slightly elongated due to the incorporation of ferrite particles into PPy.

Table 4. FTIR absorption band values and their assignment of PPy and the composite sample (other than the band values of ferrites displayed above in Table 3).

Wave number (cm^{-1}) PPy	Wave number (cm^{-1}) PPy /$Cu_{0.5}Ni_{0.5}Al_{0.3}Fe_{1.7}O_4$	Absorption peak assignment
896	887	out-of-plane stretching vibration of C–H [32]
1400	1396	C=C stretching ring of PPy [33]
1471	1473	C-N stretching vibration of PPy [33, 30]
1645	1647	Vibration band of PPy ring [32]
1724	1726	Anti-symmetrical and symmetrical vibration bands of pyrrole ring [34]

4.4 Elastic properties

In view of the widely different applications of nano-crystalline ferrites, the investigation of their elastic properties is very important because they may predict the performance of materials under stress conditions. Also, they give information about the nature of the inter-atomic forces. The Debye temperature, Θ_D, is a key quantity in Debye theory of heat capacity and it is defined as $\Theta_D = h\upsilon_D k$, where h is Planck's constant; k is Boltzmann constant and υ_D is the maximum frequency in the range of frequencies exhibited by the vibrating atoms in a solid [30]. In the case of spinel ferrites Θ_D of all samples was estimated by using the following relation [37]: $\Theta_D = \lambda c \upsilon_{AV} = 1.438\upsilon_{AV}$, where $\upsilon_{AV} = \frac{\upsilon_1+\upsilon_2}{2}$ is the average value of wavenumbers for the A-and B-site and the value of λc for the ferrite materials was taken as1.438 [35]. The elastic constants and Debye temperature of a spinel ferrite system can be deduced using the experimental XRD and IR data. The stiffness constants C_{11} and $C_{12}$are at first calculated using [35- 37]:

$$C_{11} = \frac{F}{a} \quad \text{and} \quad C_{12} = \frac{\sigma C_{11}}{1-\sigma}$$

; Where $F = \frac{F_A+F_B}{2}$ and σ is the Poisson's ratio that is a function of porosity (P) [38]:

$$\sigma = 0.324(1 - 1.043\mathrm{P}).$$

Then, in terms of these stiffness constants the elastic moduli can be evaluated [35, 38, 39]:

Bulk modulus $B = \frac{1}{3}(C_{11} + 2C_{12})$

Young's modulus $E = \frac{(C_{11}-C_{12})(C_{11}+2C_{12})}{(C_{11}+C_{12})}$

Rigidity modulus $G = \frac{E}{2(\sigma+1)}$

Moreover, the longitudinal elastic wave velocity V_L can be calculated from [30, 40]:

$$V_L = \sqrt{\frac{C_{11}}{D_X}}$$

Whereas the transverse elastic wave velocity V_S is given by:

$$V_S = \frac{V_L}{\sqrt{3}}$$

The stiffness constants, the elastic moduli, and the values of elastic wave velocities are presented in Table 5.

Table5. The stiffness constants: C_{11}, C_{12}, elastic moduli: B, G and E, elastic wave velocities: V_L and V_S and Poisson's ratio (σ)

x	C_{11}(Gpa)	C_{12}(Gpa)	B(Gpa)	E(Gpa)	G(Gpa)	$V_L(10^3$m/sec)	$V_S(10^3$m/sec)	σ
0	351	55.774	154.147	335.954	147.559	8.086	4.669	0.1371
0.1	364	55.072	158.07	349.593	154.497	8.242	4.759	0.1313
0.2	364	57.582	159.623	347.962	153.06	8.267	4.773	0.1367
0.3	367	59.797	162.142	350.136	153.556	8.335	4.812	0.1401
0.4	371	49.277	156.472	359.3	160.791	8.377	4.836	0.1173

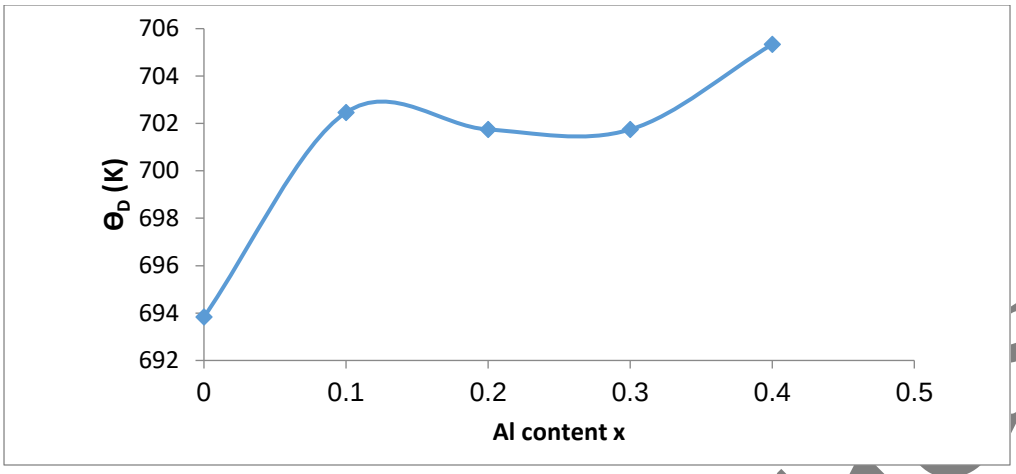

Fig.8 The relation between Debye temperature Θ_D and the Al content (x).

Fig. 8 illustrates the relation between Θ_D and the concentration of Al. It illustrates that Θ_D increases with increasing Al content, implying that an increase in rigidity of the samples occurs along with the lattice vibrations. Also, according to the specific heat theory, the increase in Θ_D means indirectly a decrease in the number of conduction electrons, and at the same time it may indicate an increase in the contribution of holes to conductivity [36, 41].

4.5 Magnetic Properties

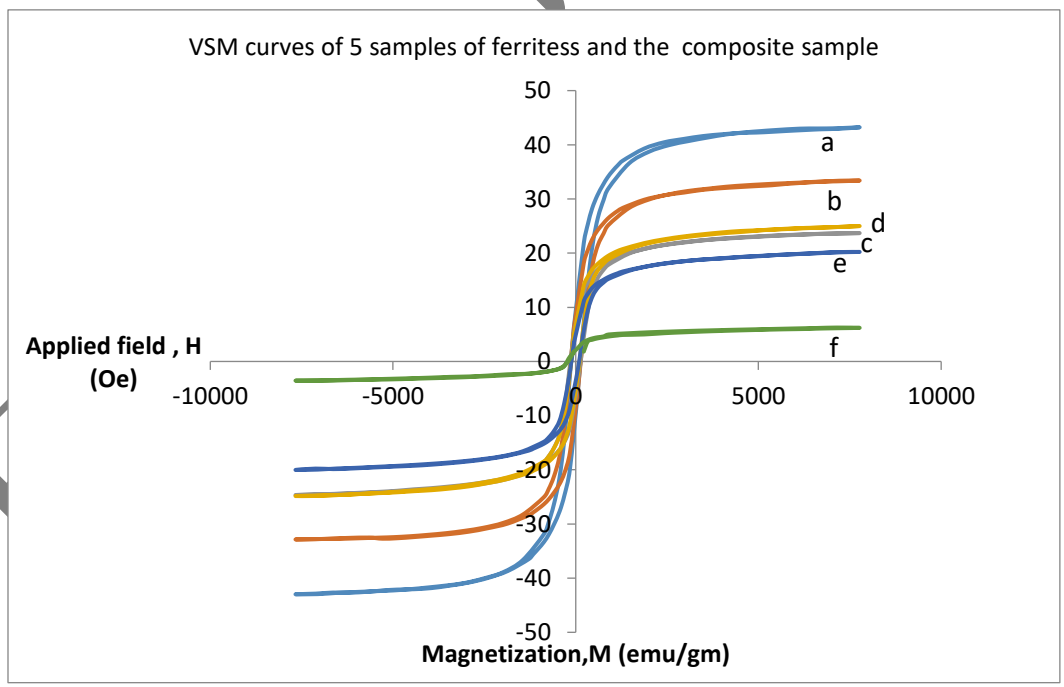

Fig.9 Hysteresis loops of : (a) $Cu_{0.5}Ni_{0.5}Fe_2O_4$, (b) $Cu_{0.5}Ni_{0.5}Al_{0.1}Fe_{1.9}O_4$, (c) $Cu_{0.5}Ni_{0.5}Al_{0.2}Fe_{1.8}O_4$, (d) $Cu_{0.5}Ni_{0.5}Al_{0.3}Fe_{1.7}O_4$, (e) $Cu_{0.5}Ni_{0.5}Al_{0.4}Fe_{1.6}O_4$ and

(f) $Cu_{0.5}Ni_{0.5}Al_{0.3}Fe_{1.7}O_4$/PPy.

The magnetic properties of the as papered $Cu_{0.5}Ni_{0.5}Al_xFe_{2-x}O_4$ nanoparticles and the composite sample $Cu_{0.5}Ni_{0.5}Al_{0.3}Fe_{1.7}O_4$ /PPy have been examined using the vibrating sample magnetometer (VSM) at room temperature. Fig.9 shows all the hysteresis loops of the samples. The samples exhibit very narrow hysteresis curves, so that they can be classified as soft magnetic materials. The coercivity (H_c), saturation magnetization (M_s) and remanent magnetization (M_r) for all samples are listed in Table 6. The observed changes in the values of M_s, H_c and M_r with increasing of Al concentrations can be explained according to the expected changes in exchange interaction between the ions at tetrahedral (A) and octahedral (B) sites in ferrites upon the variation in chemical composition [42]. The saturation magnetization decreases with the increase in Al content (x), which is quite reasonable due to the substitution of magnetic Fe^{3+} ions ($5\mu_B$) by nonmagnetic Al^{3+} ions ($0\ \mu_B$). Also, it can be seen from Table 5 that the coercivity increases slightly upon introducing Al, following an almost similar behavior reported in literature [26].

It is also noticed that the saturation magnetization in the composite sample is further lowered than those of pure ferrites; this is due to the introduction of the nonmagnetic PPy part into the sample under investigation; where PPy may separate the magnetic particles apart, disrupting the magnetic order. It is also noticed that the coercivity (H_c) value of the composite is higher compared to that of the pure Cu Ni ferrite because the PPy increases the surface anisotropy of the composite, whereas it is almost equal to the coercivity of the Al containing ferrites, indicating some similarity of introducing Al and PPy from the perspective of interruption of the magnetic order. In spite of increasing H_c with increasing both Al^{3+} ion content and PPy, its value is still low enough for application. since the low coercivity of the samples is required in important devices and applications which depend on soft magnetic materials such as switching devices and high frequency transformers [14].

Table 6 The values of saturation magnetization (Ms), remanent magnetization (Mr), coercivity (Hc), and Squareness:

Sample	M_s (emu/g)	M_r (emu/g)	H_c (G)	Squareness (M_r/M_s)
$Cu_{0.5}Ni_{0.5}Fe_{2-x}O_4$	43.228	9.5	120	0.220
$Cu_{0.5}Ni_{0.5}Al_{0.1}Fe_{1.9}O_4$	33.396	8.5	140	0.255
$Cu_{0.5}Ni_{0.5}Al_{0.2}Fe_{1.8}O_4$	23.695	6.5	140	0.274
$Cu_{0.5}Ni_{0.5}Al_{0.3}Fe_{1.7}O_4$	23.695	6.5	140	0.274
$Cu_{0.5}Ni_{0.5}Al_{0.4}Fe_{1.6}O_4$	20.216	4.45	101	0.220
$Cu_{0.5}Ni_{0.5}Al_{0.3}Fe_{1.7}O_4$/ PPy	6.260	1.2	140	0.192

5. Conclusions

Citrate precursor technique could provide small sized nanoparticles of Cu0.5Ni0.5AlxFe2-xO4 with various compositions. The formation of spinel ferrites without unwanted phases was confirmed by X-ray diffraction analysis. The IR spectra confirmed the formation of both ferrites and PPy. The study of increase of the Al content (x) in the Cu Ni ferrite shows that the lattice constant and theoretical density decrease due to the difference in ionic radii and molar mass of both aluminum ions and iron ions respectively. PPy/Cu0.5Ni0.5Al0.3Fe1.7O4 composite sample could be successfully synthesized by the use of in situ chemical polymerization method. The SEM images confirm the nanoscale diameter of Cu0.5Ni0.5Al0.3Fe1.7 O4 particles in both ferrite and composite. The substitution of Fe3+ ions by Al3+ ions in the samples has decreased the saturation magnetization, in agreement with literature. The coercivity of the ferrite containing Al and the composite are almost equal, indicating some similarity of the effect of introducing Al and PPy to the Cu Ni ferrite from the perspective of interruption of ferrimagnetic order. Due to the low coercivity of the samples, these materials may be good candidates for important devices and applications which depend on soft magnetic materials such as switching devices and high frequency transformers.

References

[1] S.A. Saafan, T.M. Meaz, E.H. El-Ghazzawy, Study of DC conductivity and relative magnetic permeability of nanoparticle NiZnFe2O4/PPy composites, J. Magn. Magn. Mater. 323 (2011) 1517–1524.

[2] M.A.Darwish, S.A.Saafan, D.El-Kony, N.A.Salahuddin, Preparation and investigation of dc conductivity and relative permeability of epoxy/Li–Ni–Zn ferrite composites, J. Magn. Magn. Mater. 385(2015)99–106.

[3] M. K. Dasa, M.A. Zubair, H. Tanaka, A.K.M. Akther Hossain, An experimental insight of the multiferroic properties of magnetoelectrically Coupled *x*LNCZFO + (1−*x*)BSTDO composites, J. Magn. Magn. Mater. 502 (2020) 166449.

[4] J. Alam, U. Riaz, Sh. Ahmad, Effect of ferrofluid concentration on electrical and magnetic properties of the Fe3O4/PANI nanocomposites, J. Magn. Magn. Mater. 314 (2007) 93–99.

[5] A.M. Abdeen, Electric conduction in Ni-Zn ferrites, J. Magn. Magn. Mater. 185(1998) 199–206.

[6] S.R. Shannigrahi, K.P. Pramoda, F.A.A. Nugroho, Synthesis and characterizations of microwave sintered ferrite powders and their composite films for practical applications, J. Magn. Magn. Mater. 324 (2012) 140–145.

[7] A. Hassana, M. A. Khan, M. Shahid, M. Asghara, I. Shakir, Sh. Naseem, S. Riaz, M. F. Warsi, NanocrystallineZn$_{1_x}$ Co$_{0.5x}$Ni$_{0.5x}$ Fe$_2$O$_4$ ferrites: Fabrication via co- precipitation route with enhanced magnetic and electrical properties, J. Magn. Magn. Mater. 393 (2015) 56-61.

[8] R. Felhi, K. Riahi, H. Omrani, M. Koubaa, W. Cheikhrouhou Koubaa, A. Cheikhrouhou, Assessment of the critical behavior near the FM to PM phase transition in cubic Ni$_{0.3-x}$Cu$_x$Zn$_{0.7}$Fe$_2$O$_4$ spinel ferrite, J. Magn. Magn. Mater. 503 (2020) 166531.

[9] A. Bajorek, B. Liszkab, B. Szostak, M. Pawlyta, Microstructure and magnetism of Ni0.5Zn0.5Fe2O4/MWCNTs nanocomposites, J. Magn. Magn. Mater. 503 (2020) 166634.

[10] M.A. Ahmed, M.A. E1 Hiti, M.M. Mosaad, S.M. Attia, AC Conductivity in Cu- Cr ferrites, J. Magn. Magn. Mater. 146 (1995) 84-88.

[11] J. Jadhav, S. Biswas, A.K. Yadav, S.N. Jha, D. Bhattacharyya, Structural and magnetic properties of nanocrystalline Ni-Zn ferrites: In the context of cationic distribution, j. Alloys. Compd.696 (2017)28-41.

[12] G. R. Kumar, K. V. Kumar, Y.C. Venudhar, Synthesis, Structural and Magnetic Properties of Copper Substituted Nickel Ferrites by Sol-Gel Method, J. Mater. Sci. Appl. 3 (2012) 87-91.

[13] S.S. Ata-Allah, M.K. Fayek, Effect of Cu substitution on conductivity of Ni–Al ferrite, j. Phys. Chem. Soli. 61 (2000) 1529–1534.

[14] E.H. El-Ghazzawy, and S.N. Alamri, NiCr$_x$Fe$_{2-x}$O$_4$ ferrite nanoparticles and their composites with polypyrrole: synthesis, characterization and magnetic properties, j. Bull. Mater.38 (2015) 915–924.

[15] E. Agouriane, B. Rabi, A. Essoumhi, A. Razouk, M. Sahlaoui1, B. F. O. Costa, M. Sajieddine, Structural and magnetic properties of CuFe$_2$O$_4$ ferrite nanoparticles synthesized by co-precipitation, J. Mater. Environ. Sci. 7 (11) (2016) 4116-4120.

[16] S. M. Hoque, Md. A. Choudhury, Md. F. Islam, Characterization of Ni–Cu mixed spinel ferrite, J. Magn. Magn. Mater. 251 (2002) 292–303.

[17] A. Yussuf, M. Al-Saleh, S.Al-Enezi, and G. Abraham, Synthesis and Characterization of Conductive Polypyrrole: The Influence of the Oxidants and Monomer on the Electrical, Thermal, and Morphological Properties, Int. J. Polym. Sci. (2018) 1-8, https://doi.org/10.1155/2018/4191747.

[18] A. Kassim, Z. Btebasar, H. E. Mahmud, Effects of preparation temperature on the conductivity of polypyrrole conducting polymer, j. Chem. Sci. 114 (2002) 155–162.

[19] O. Yavuza, M. K. Ram, M. Aldissi, P. Poddar, H. Srikanth, Polypyrrole composites for shielding applications, j. Synth. Metal. 151 (2005) 211–217.

[20] P. Gairola, L.P. Purohita, S.P. Gairola, P. Bhardwaj, Sh. Kaushik, Enhanced electromagnetic absorption in ferrite and tantalum pent oxide based polypyrrole nanocomposite, J, Prog. Nat. Sci-Mater. 29 (2019) 170–176.

[21] I. V. K. Viswanath, Y. L. N. Murthy, K. Raotata, R. Singh, Synthesis and Characterization of nano Ferrites by Citrate Gel Method, J. Chem. Sci. 11(2013) 64-72.

[22] B. K. Kumar, D. Ravikumar, D. Ravinder, Ch. A. Lincoln, Preparation and Structural Properties of Manganese Substituted cobalt Nano Ferrites By Citrate-Gel Auto Combustion Method, J. appl. Chem. 8 (2015) 23-29.

[23] J. K.Mathad, R.M.V.G.K. Rao, Studies on Highly Conducting Polypyrrole/Fe3O4 Nanocomposites, J. Polym. Compd. (2011p) DOI 10.1002/pc.21167.

[24] T.M.EL-Alaily, M.K.EL-Nimr, S.A. Saafan, M.M.Kamel, T.M.Meaz, S.T.Assar, J. Magn. Magn. Mater. 386 (2015) 25-30.

[25] B. R. Babu, M.S.R. Prasad, K.V. Ramesh, Y. Purushotham, Structural and Magnetic properties of $Ni_{0.5}Zn_{0.5}Al_xFe_{2\_x}O_4$ nano ferrite system, J. Mater .Chem. phys.148 (2014) 585-591.

[26] A. A. Birajdar, S. E. Shirsath, R. H. Kadam, M. L. Mane, D. R. Mane, and A. R. Shitre, Permeability and magnetic properties of Al^{3+} substituted $Ni_{0.7}Zn_{0.3}Fe_2O_4$ nanoparticles, J. Appl. Phys. 112, 053908 (2012); doi: 10.1063/1.4748959.

[27] E.H. El-Ghazzawy, M.A. Amer, Structural, elastic and magnetic studies of the as-synthesized $Co_{1\_x}Sr_xFe_2O_4$ nanoparticles, J. Alloy. Compd. 690 (2017) 293-303.

[28] M.A. Amer, A. Matsuda, G. Kawamura, R. El-Shater, T. Meaz, F. Fakhry, Characterization and structural and magnetic studies of as-synthesized $Fe^{2+}Cr_xFe_{(2-x)}O_4$ nanoparticles, J. Magn. Magn. Mater. 439 (2017) 373–383.

[29] K. Atrak, A. Ramazani, S. T. Fardood, Eco-friendly synthesis of $Mg_{0.5}Ni_{0.5}Al_xFe_{2-x}O_4$ magnetic nanoparticles and study of their photocatalytic activity for degradation of direct blue 129 dye, J. Photoch. Photobio. A. 382 (2019) 111942.

[30] E.H. El-Ghazzawy, Effect of heat treatment on structural, magnetic, elastic and optical properties of the co-precipitated $Co_{0.4}Sr_{0.6}Fe_2O_4$, J. Magn. Magn. Mater. 497 (2020) 166017.

[31] O. Yavuz, M. K. Ram, M. Aldissi, P. Poddar, H. Srikanth, Polypyrrole composites for shielding applications, J. Synth. Met. 151 (2005) 211–217.

[32] H. Eisazadeh, Studying the Characteristics of Polypyrrole and its Composites, J. chem. 2 (2007) 67-74.

[33] A. Elahi, N. A. Niaz, M. S. Awan, A. Shakoor, K. Mahmood, and Y. Khan, Structural, Electrical, and Magnetic Properties of Polypyrrole–$Zn_{0.5}Ni_{0.45}Mn_{0.05}Fe_2O_4$ Nanocomposites Prepared by In Situ Chemical Polymerization, J. Polym. Sci. 57 (2015) 738–749.

[34] A. Elahi, A. Shakoor, M. Irfan, K. Mahmood, N. A. Niaz, M. S. Awan,T. Bashi, Polypyrrole and its nanocomposites with $Zn_{0.5}Ni_{0.4}Cr_{0.1}Fe_2O_4$ferrite: preparation and electromagnetic properties, J. Mater. Sci.27 (2016) 6964–6973.

[35] S.M. Patange, S. E. Shirsath, K. S. Lohar, S. G. Algude, S. R. Kamble, N. Kulkarni, D.R. Mane, K. M. Jadhav, Infrared spectral and elastic moduli study of $NiFe_{2-x}Cr_xO_4$ nanocrystalline ferrites, J. Magn. Magn. Mater. 325 (2013) 107–111.

[36] M.A. Amer, Structural and magnetic studies of the $Co_{1+x}Ti_x$ Fe $_{2(1-x)}O_4$ ferrites, J. Magn. Magn. Mater. 426 (2017) 771–778.

[37] M.A. Amer, T.M.Meaz, S.S. Attalah, A.I. Ghoneim, Structural phase transformation of as-prepared Mg–Mn nanoferrites by annealing temperature, J. Mate. Charact.110 (2015) 197–207.

[38] M.A.Amer, T.Meaz, S.Attalah, F.Fakhry, Influence of heat treatment on magnetic, structural and elastic properties of as-prepared Mg-nanoferrites, J. Magn. Magn. Mater. 401(2016)150–158.

[39] S.S. Bhatu, V. K. Lakhani, A. R. Tanna, N. H. Vasoya, J. U. Buch, P. U. Sharma, U. N. Trivedi, H. H. Hoshi, K. B. Modi, Effect of Nickel substitution on structural, infrared and elastic properties of lithium ferrite, J. Pure. Appl. Phys. 45 (2007) 596-608.

[40] S. A.Mazen and T. A. Elmosalami, Structural and Elastic Properties of Li-Ni Ferrite, ISRN Condens. Matter. Phys. 2011 (2011) 1–9, https://doi.org/10.5402/2011/820726.

[41] M.A. Amer, T.M. Meaz, A. Hashhash, S.S. Attalah, A.I. Ghoneim, Structural properties and magnetic interactions in Sr-doped Mg-Mn nanoparticle ferrites, J. Materials Chemistry and Physics 162 (2015) 442-451.

[42] A. M. El Nahrawy, H. Salah El-Deen, A.A. Soliman, W. M.M. Mosa, Crystallographic and Magnetic Properties of Al^{3+}co-doped $NiZnFe_2O_4$ Nano-particles Prepared by Sol-gel Process, J. Chem. 62 (2019) 525 - 532.